Biosensors and Bioelectronics 92 (2017) 1–7

Contents lists available at ScienceDirect

Biosensors and Bioelectronics

journal homepage: www.elsevier.com/locate/bios

Label-free immunosensor based on hyperbranched polyester for specific detection of α-fetoprotein

Yanlian Niu, Tian Yang, Shangshang Ma, Fang Peng, Meihui Yi, Mimi Wan, Chun Mao*, Jian Shen*

National and Local Joint Engineering Research Center of Biomedical Functional Materials, Jiangsu Key Laboratory of Biofunctional Materials, School of Chemistry and Materials Science, Nanjing Normal University, Nanjing 210023, China

ARTICLE INFO

Keywords:
Hyperbranched polyester
Electrochemical immunosensor
Ultra-stability
Label-free
α-Fetoprotein

ABSTRACT

A novel label-free immunosensor based on hyperbranched polyester nanoparticles with nitrite groups (HBPE-NO_2), which were synthesized through a simple one-step chemical reaction, was first developed for specific detection of α-fetoprotein (AFP), the tumor marker for liver cancer. The obtained HBPE-NO_2 nanoparticles (NPs) were characterized by the proton nuclear magnetic resonance spectroscopy (^{1}H NMR), X-ray photoelectron spectroscopy (XPS) and X-ray diffraction (XRD). And the fabricated process of immunosensor was investigated by attenuated total reflection Fourier-transform infrared spectra (ATR-FTIR), static water contact angles, scanning electron microscope (SEM), cyclic voltammetry (CV) and electrochemical impedance spectroscopy (EIS). The electrochemical performances of the AFP immunosensor were studied. Results indicated the prepared HBPE-NO_2-modified immunosensor showed excellent electrochemical properties and satisfactory accuracy for the detection of AFP of the real clinical samples that attributed to the properties of the HBPE-NO_2 NPs, which had nanosized structure to increase the specific surface area and unique chemical reactivity for loading capacity of protein molecules. Construction of biosensors using the structure and properties of hyperbranched molecules will offer ideal electrode substrates, which provided more possibilities for the design of biosensor.

1. Introduction

Alpha-fetoprotein (AFP), an important tumor marker, is widely used for the diagnosis of patients with germ cell tumors and hepatocellular carcinoma (Alpert et al., 1971; Okuda, 1986; Wang and Xie, 1998), and its concentration is below 20 ng/mL in healthy human serum while much higher in liver cancer patient serum (Xie et al., 2016; Zhou et al., 2015). Therefore, the reliable detection of AFP is significant for the early clinical diagnosis and the long-term treatment (Li et al., 2015). In recent years, numerous novel technologies were developed and applied for AFP detection (Chen et al., 2012; Darwish et al., 2013; Law et al., 2011; Xiao et al., 2014). Electrochemical bioanalytical technique, with a number of virtues such as simple preparation and operation, high sensitivity and selectivity, wide detection range and so forth, has become increasingly important in biological assays (Cui et al., 2016). Particularly, electrochemical label-free immunosensors have been considered to be one of the most promising methods to quantitatively detect AFP owing to their specific advantages, such as low price, low detection limits, fast response, and easy handling (Kavosi et al., 2014).

For the construction of an excellent label-free electrochemical immunosensor, it is crucial that the immobilization of biomolecules onto the electrode surface should be which could ensure the activity of antibody without affected (G.L Wang et al., 2009; J. Wang et al., 2009). Therefore, the electrode substrate should provide a large surface area to immobilize more antibodies and also offer good conductivity in order to assist the electron transfer, as well as stability and without biological toxicity. So how can design and prepare the ideal electrode substrate that can immobilize antibodies sufficiently and effectively for electrochemical immunosensor became the key to this research work.

Hyperbranched polymers (HBP) have attracted more and more attention because of the special architecture and properties that include their three-dimensional shapes, high density of end-groups, nanosized effect, good solubility, etc (Ahmed and Narain, 2012; Magnusson et al., 2000; Karpagam and Guhanathan, 2010; Ding et al., 2012). Further, owing to the multifunctionality in HBP, their properties can be adjusted to a great degree by various chemical modification of the large number of functional end-groups for special

* Corresponding authors.
E-mail addresses: maochun@njnu.edu.cn (C. Mao), jshen@njnu.edu.cn (J. Shen).

http://dx.doi.org/10.1016/j.bios.2017.01.069
Received 1 December 2016; Received in revised form 23 January 2017; Accepted 31 January 2017
Available online 01 February 2017
0956-5663/

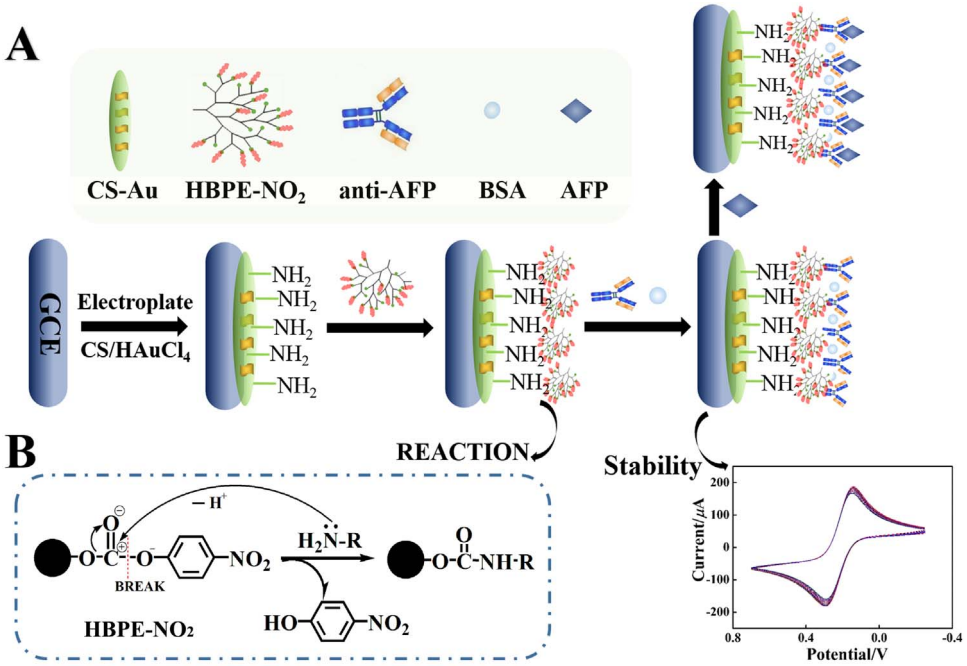

Scheme 1. (A) Schematic illustration of the fabrication process of the AFP biosensor; (B) The nucleophilic substitution reaction mechanism between HBPE-NO_2 NPs and primary amines (-NH_2).

purposes, which made the HBP have been used extensively in diverse fields, such as coatings, additives, biomedical fields, and photoelectric materials (Gao and Yan, 2004; Seiler et al., 2004; Hong et al., 2008; Zagar et al., 2006; Kontoyianni et al., 2008; Sun et al., 2014).

In this case, *p*-nitrophenyl oxycarbonyl group-terminated hyperbranched polyester (HBPE-NO_2), obtained from hyperbranched polyester with terminal hydroxyl groups (HBPE-OH) that modified by *p*-nitrophenyl chloroformate containing active esters group (-O-COO-), which can react with primary amine (-NH_2) of chitosan (CS) and anti-AFP in situ, respectively. Based on this, a novel electrochemical immunoassay biosensor was proposed and its biosensing performance was investigated.

2. Experimental section

2.1. Synthesis of HBPE-NO_2 nanoparticles (NPs)

As shown in Scheme S1, HBPE-NO_2 was synthesized through one-step chemical reaction. 1.0 g HBPE-OH (aliphatic hyperbranched polyester with terminal -OH group) (Scheme S1A) was dissolved in anhydrous tetrahydrofuran (THF, 100 mL), then 10 mL anhydrous THF containing *p*-nitrophenyl chloroformate (2.0 g, 9.9 mmol) was added dropwise with the presence of an excess of triethylamine (TEA, 1.5 mL). And the mixture was allowed to continue to react about 12 h with stirring at room temperature (Scheme S1B). After the reaction, a yellowish opacity solution was formed finally (Hu and Ji, 2011), and then the resulting solution was filtered and concentrated to about 10 mL through rotary evaporation. The final product was obtained by precipitation from diethyl ether, then redissolved in THF and reprecipitated from diethyl ether again, the reprecipitation procedure was repeated three times to remove the residual *p*-nitrophenyl chloroformate and dried in a vacuum.

2.2. Fabrication of the HBPE-NO_2 NPs modified biosensor

Glassy carbon electrode (GCE) was used as base electrode. Prior to modification, it was polished to a mirror finish using 0.3 and 0.05 μm alumina slurry, respectively, and rinsed thoroughly with distilled water between each polishing step (Sun et al., 2013). After that, the mirror-like electrode was sonicated in pure ethanol and distilled water about 5 min, respectively, and allowed to air-dry at room temperature.

The preparation procedure of AFP biosensor was shown in Scheme 1. Firstly, the GCE was electrodeposited with CS and hydrogen tetrachloroaurate (III) trihydrate ($HAuCl_4 \cdot 3H_2O$, 99.9%) mixture containing 2 mL of 1 g/L CS (1% acetic acid as solvent) and 2 mL of 500 mg/L $HAuCl_4$ solution by applying a constant potential of −1.5 V for 180 s, then the modified GCE were rinsed with distilled water to obtain the CS-Au NPs modified electrode (CS-Au/GCE) (Sun et al., 2014). The CS-Au/GCE was soaked in 8 mL of 0.1 mg/mL HBPE-NO_2 solution (dispersed in distilled water and sonicated well) for 15 min and then rinsed with distilled water to remove the unreacted HBPE-NO_2 (Scheme 1A). Thus, the HBPE-NO_2 NPs were immobilized by electrostatic absorption and in situ chemical reaction (Scheme 1B), and the obtained (HBPE-NO_2)/CS-Au/GCE was stored at 4 °C before use. *p*-Nitrophenol, the byproduct of the chemical reaction could be eliminated simply by immersion in distilled water mentioned above, which was a necessary step to ensure the activity of anti-AFP that will be grafted next step was not affected by the byproduct.

Next, AFP/anti-AFP/(HBPE-NO_2)/CS-Au/GCE biosensor was obtained easily by a three-step modified process. Firstly, the prepared (HBPE-NO_2)/CS-Au/GCE was immersed into 10 mL solution of anti-AFP (200 ng/mL, PBS, pH 7.4) for 15 min, then the modified GCE was drawn out and rinsed thoroughly with PBS subsequently, and air-dry at room temperature.

And then, the anti-AFP/(HBPE-NO_2)/CS-Au/GCE was blocked the possible remaining active sites against the nonspecific adsorption by 2% bovine serum albumin (BSA) for 1 h. Finally, the modified electrodes were incubated in 10 mL AFP standard solutions of various concentrations (0.1 mol/L PBS, pH 7.4) for 15 min, followed by washing with PBS. Thus, the resulting AFP/anti-AFP/(HBPE-NO_2)/CS-Au/GCE was recorded to produce the detection signal corresponding to the presence of an analyte, and the obtained AFP/anti-AFP/(HBPE-NO_2)/CS-Au/GCE was stored at 4 °C before use.

2.3. Electrochemical measurements

Cyclic voltammetry (CV) was performed over the potentials between −0.2 V~0.7 V. The differential pulse voltammetry (DPV) was

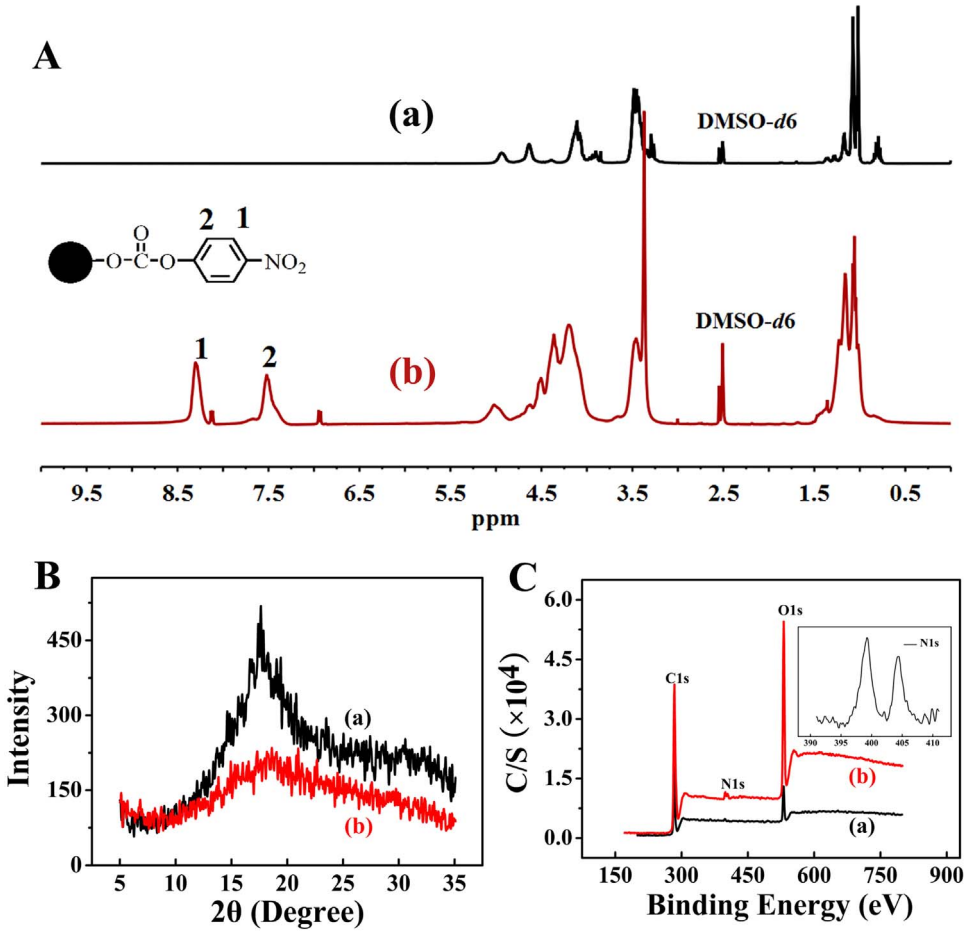

Fig. 1. (A) The ^{1}H NMR spectra, (B) XRD patterns and (C) XPS, wide scan of (a) HBPE-OH and (b) HBPE-NO_2. The inset in Fig (C) was N1s of core-level spectrum.

carried out as amplitude of 0.05 V, pulse width of 0.05 s and voltage range from −0.2 to 0.6 V. Electrochemical impedance spectroscopy (EIS) measurement is a powerful technique to monitor the changes occurred at electrode surfaces (Feng et al., 2012), herein the measurements were operated in the frequency range of 1 Hz–100 kHz with 5 mV AC amplitude, quiet time: 2 s.

3. Results and discussion

3.1. HBPE-NO_2 composite preparation and biosensor fabrication

3.1.1. Characterization of HBPE-NO_2 NPs

As shown in Fig. 1A, in the proton nuclear magnetic resonance (^{1}H NMR) spectrum of HBPE-NO_2, two new proton peaks (peaks 1 and 2) appeared at 7.52 ppm and 8.31 ppm assigned to the protons of phenyl ring from the attached *p*-nitrophenyl oxycarbonyl group compared with the ^{1}H NMR spectrum of HBPE-OH (Han et al., 2013; Gündüz et al., 2014). Furthermore, in the Fourier-transform infrared spectrum (FTIR) of HBPE-NO_2, the strong peak at 1739 cm^{-1} was attributed to the -COO- asymmetrical vibration from the HBPE-OH, and the absorption peaks at 1600 cm^{-1} and 1527 cm^{-1} that were not observed on that of HBPE-OH were identified as characteristic peaks of phenyl ring (Wang et al., 2013, 2014; Lu et al., 2005) (Fig. S1). Results indicated that the reactive ester groups (-O-COO-) have been grafted onto the terminal group of HBPE-OH successfully. The X-ray diffraction (XRD) and X-ray photoelectron spectroscopy (XPS) were adopted to further evidence the structure and components of HBPE-OH and HBPE-NO_2. As shown in Fig. 1B, a broad non-crystalline peak in the region of 2θ=10–35° was attributed to the major peak of the HBPE-OH (2θ=17.5°). Meanwhile, the diffraction intensity of HBPE-NO_2 NPs decreased compared with the HBPE-OH, which was assigned to the successful nitroso-terminated modification of HBPE-OH NPs (Sun et al., 2015). XPS spectra of the HBPE-NO_2 NPs contained C1s (283.4 eV), O1s (531.1 eV), N1s (399.4 eV, 404.4 eV) peaks, however, N1s peaks weren't observed in XPS spectrum of HBPE-OH NPs (Fig. 1C).

3.1.2. Surface characterization of the biosensor

The chemical structures of CS-Au/GCE and HBPE-NO_2/CS-Au/GCE surface were monitored by attenuated total reflection Fourier-transform infrared spectra (ATR-FTIR). In the case of the GCE surface electrodeposited with CS-Au, the absorptions at 3391 cm^{-1} and 2933 cm^{-1} were attributed to the -OH and -CH(OH)-CH(OH)- group from CS, respectively. Furthermore, the peaks at 1637 cm^{-1} and 1520 cm^{-1} were attributed to the stretching vibration of amide I and amide II of the amido bond from CS (Fig. 2A (a)) (Mucha et al., 1999; Socrates, 1994; Kolhe and Kannan, 2003). The spectrum of HBPE-NO_2 NPs grafted onto CS-Au/GCE showed strong peak at 1736 cm^{-1}, which can be associated with -COO- asymmetrical vibration (Fig. 2A (b)) (Pérez-Donoso et al., 2012; Pilla et al., 2013). In addition, the absorption peaks at 1614 cm^{-1} and 1521 cm^{-1} can be assigned to the overlap between amido bond of CS and characteristic peaks of phenyl ring from the *p*-nitrophenyl oxycarbonyl. These peaks confirmed that the HBPE-NO_2 NPs were successfully grafted onto the CS-Au/GCE by the electrostatic interaction result from the negatively charged of HBPE-NO_2 NPs (−36.9 mV) (Fig. S2) and the chemical reaction (Scheme 1B). The next grafting anti-AFP on the HBPE-NO_2 NPs will be proved by CV and EIS.

As shown in Scheme 1B, while the lone pair electrons on the N atom from -NH_2 of CS and anti-AFP attack the quaternary carbon atoms

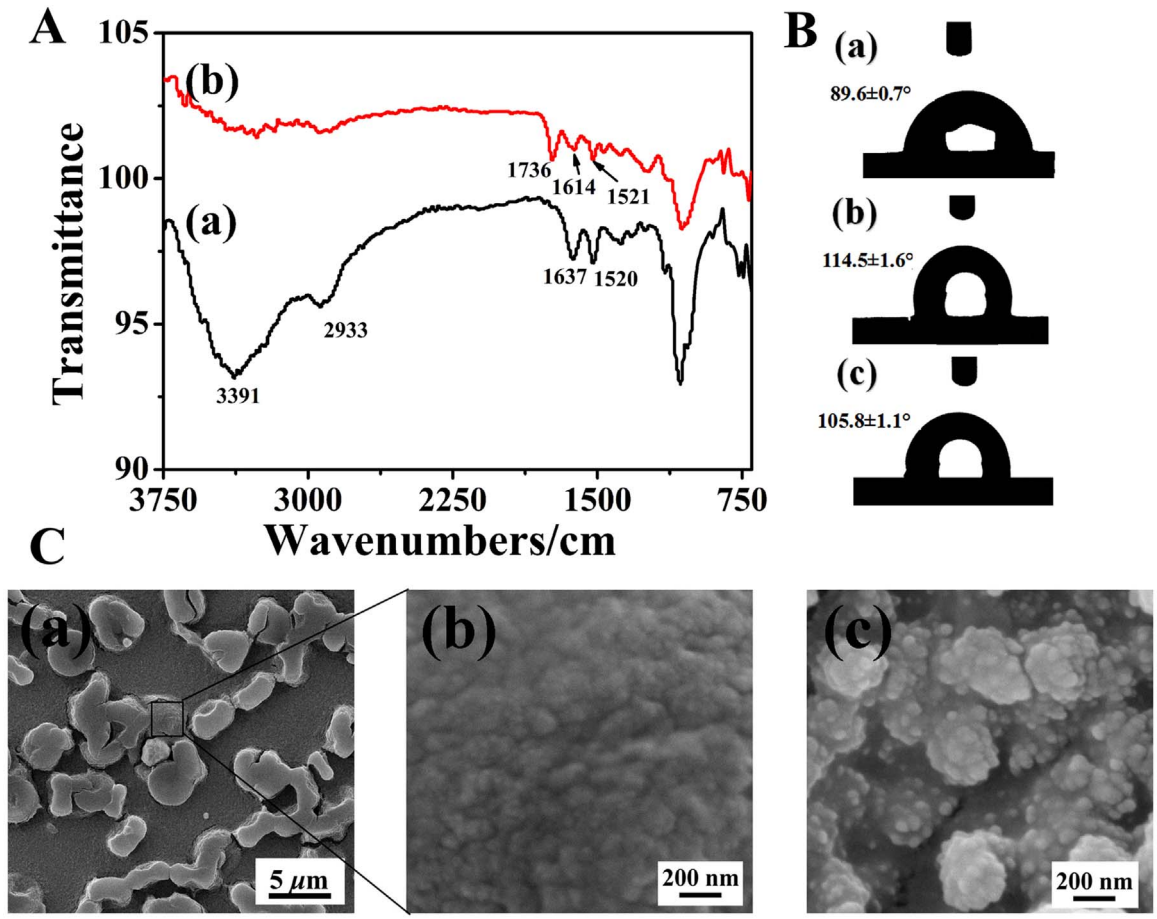

Fig. 2. (A) ATR-FTIR spectra of (a) CS-Au/GCE and (b) HBPE-NO_2/CS-Au/GCE; (B) The static water contact angles of (a) GCE, (b) CS-Au/GCE and (c) HBPE-NO_2/CS-Au/GCE surface and (C) The morphologies of the (a) CS-Au/GCE, (b) Drawing of partial enlargement of CS-Au/GCE and (c) HBPE-NO_2/CS-Au/GCE surface.

(electron-deficient) from -O-COO- of HBPE-NO_2, the nucleophilic substitution reaction took place between -NH_2 (CS and anti-AFP) and -O-COO- of HBPE-NO_2. The explanation and experimental verification for the interaction happened between HBPE-NO_2 and anti-AFP were also provided by ultraviolet visible (UV–vis) absorption spectra (Fig. S3).

For further certifying the surface modification process, static water contact angle measurements were taken at ambient temperature employing the sessile drop method. The contact angle results in Fig. 2B showed the evolution of the GCE modified process, compared to the pristine GCE, the contact angle of the CS-Au/GCE surface was increased from about 89.6 ± 0.7° to about 114.5 ± 1.6°, owing to the fact that surface roughness increased after electrodeposited CS-Au NPs (G.L. Wang et al., 2009; J. Wang et al., 2009; Ellinas et al., 2016). The immobilization of HBPE-NO_2 NPs decreased the surface contact angle of the CS-Au/GCE with contact angle about 105.8 ± 1.1° because of the existence of hydrophilic group (-NO_2), but the HBPE-NO_2/CS-Au/GCE surface was still hydrophobic (contact angle > 90°), which due to the hyperbranched polyester skeleton exhibited hydrophobicity and especially, the 3D micro-environment on the surface of HBPE-NO_2/CS-Au/GCE.

Scanning electron microscopy (SEM) was performed to estimate the morphology of the HBPE-NO_2/CS-Au/GCE biosensor surface. Typical SEM photographs showed that CS-Au NPs were well dispersed upon the GCE surface, which was resulted in the large roughness (Fig. 2C), that was why the increasing of contact angle compared to the GCE. In addition, the morphology of HBPE-NO_2/CS-Au/GCE surface was uniform nanosized particles with favorable dispersibility (Fig. 2C), which was attributed to the micellar behavior of HBPE-NO_2 NPs with an average diameter of 200 nm (Fig. S4) when incubating with CS-Au/GCE. These results indicated that the GCE surface was modified by CS-Au and HBPE-NO_2 NPs successfully. At the same time, the nanosized effect of HBPE-NO_2 NPs with abundant end-groups increased the specific surface area of CS-Au/GCE, which were beneficial for the anti-AFP grafting.

3.2. Electrochemical characterization of the immunosensor

The fabrication process of the lable-free immunosensor was characterized by CV and EIS to record the changes of the electrode behavior before and after each modification step. As shown in Fig. 3A, it was observed that the CS-Au/GCE possessed the biggest peak current (curve a). Stepwise modification on the CS-Au/GCE was along with the decreasing in amperometric response. After the CS-Au film electrode was functionalized with HBPE-NO_2 NPs, the peak current of CS-Au/GCE was greatly decreased owing to the poor conductivity of HBPE-NO_2 NPs (curve b). Moreover, three-dimensionally HBPE-NO_2/CS-Au/GCE electrode had a much larger effective surface area, which was advantage of the anti-AFP molecules grafting. Thus, when anti-AFP (curve c) and AFP (curve d) immobilized on the electrode surface in sequence, the peak currents of the redox couple decreased further on account of the obstructed electron transfer taking place at electrode surface. In another hand, the amperometric response of AFP/anti-AFP/(HBPE-NO_2)/GCE (curve e) was the weakest compared with the other modified electrode, thereby demonstrating the good conductivity of electrodeposited Au NPs.

EIS is an effective tool for studying the interface properties of surface-modified electrodes, the typical impedance spectrum is pre-

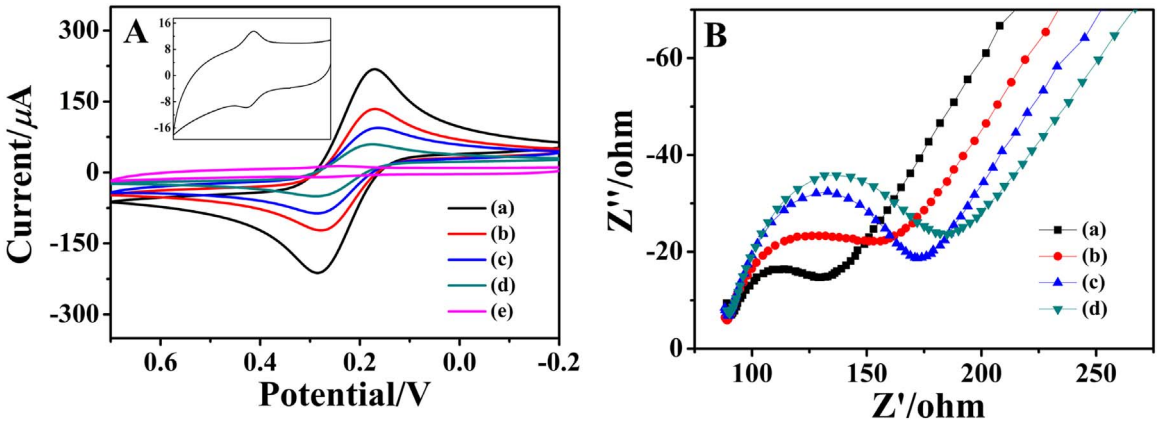

Fig. 3. (A) CV curves, scan rate: 0.1 V/s and (B) EIS of different modified electrodes in 0.1 mol/L PBS (pH 7.4) solution containing 0.1 mol/L KCl and 5 mmol/L $Fe(CN)_6^{3-}/Fe(CN)_6^{4-}$, (a) CS-Au/GCE, (b) (HBPE-NO_2)/CS-Au/GCE, (c) anti-AFP/(HBPE-NO_2)/CS-Au/GCE, (d) AFP/anti-AFP/(HBPE-NO_2)/CS-Au/GCE and (e) AFP/anti-AFP/(HBPE-NO_2)/GCE. Inset: enlargement CV curves of (e).

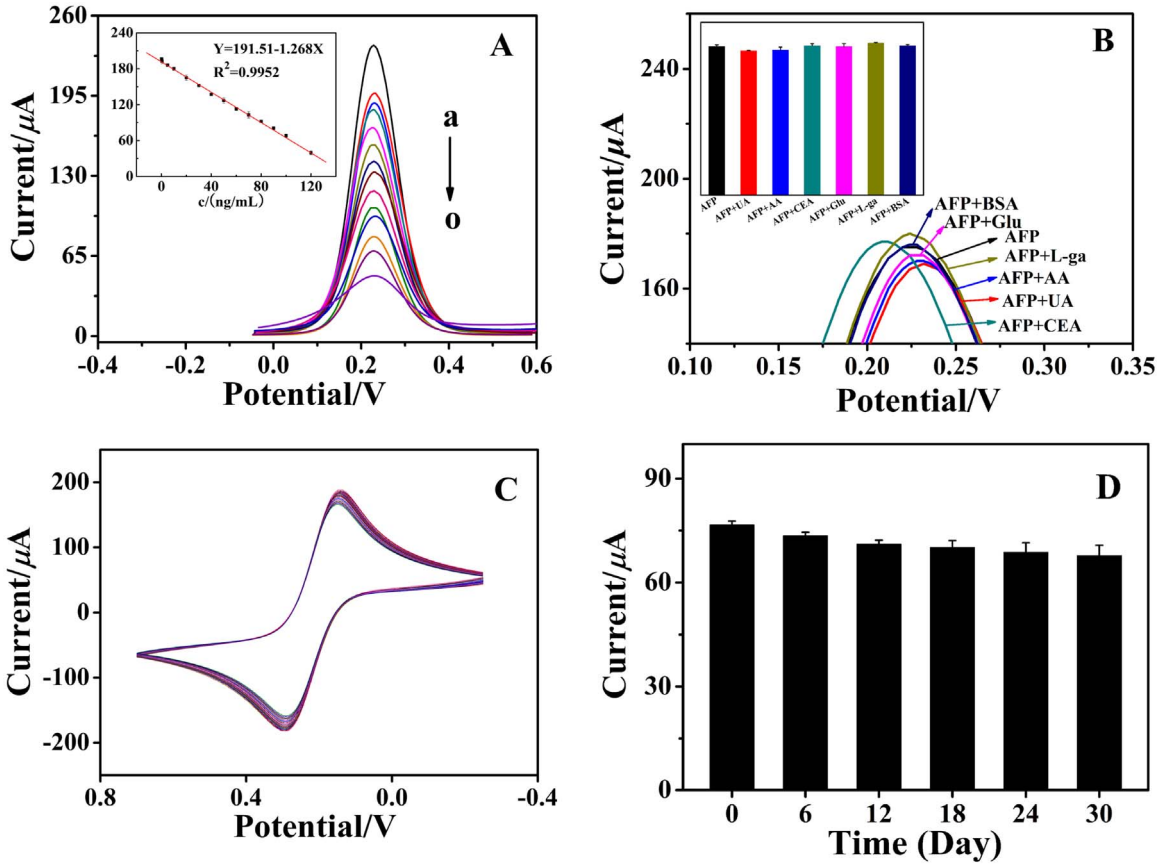

Fig. 4. (A) The DPV plots of different AFP concentration obtained at AFP/anti-AFP/(HBPE-NO_2)/CS-Au/GCE immunosensor ((a) 0, (b) 0.1, (c) 0.5, (d) 5, (e) 10, (f) 20, (g) 30, (h) 40, (i) 50, (j) 60, (k) 70, (l) 80, (m) 90, (n) 100, and (o) 120 ng/mL). Inset: calibration plots upon the addition of varying amounts of AFP; (B) The specificity of the sensor was investigated by DPV in the presence of various interfering antigens, inset: the corresponding histogram (20 ng/mL AFP, and 100 ng/mL UA, AA, CEA, Glu, L-ga, BSA); (C) CVs of anti-AFP/(HBPE-NO_2)/CS-Au/GCE at 40 cycles and (D) The charge storage capacity of AFP/anti-AFP/(HBPE-NO_2)/CS-Au/GCE was investigated by DPV stored at 4 ℃. Error bars represent the standard deviations of three repeated determinations.

sented in the form of the Nyquist plot, which is composited of the semicircle portion at higher frequencies and the linear portion at lower frequencies (Kilic et al., 2015; Chiriacò et al., 2015). The semicircle diameter in the impedance spectrum can be quantified as the charge-transfer resistance (Rct). This resistance controls the electron-transfer kinetics of the redox probe at the electrode interface (Sun et al., 2012). Therefore, Rct can be used to describe the interface properties of the electrode. Its value varies with different substances adsorbed onto the electrode surface. Fig. 3B showed the impedance spectra observed upon the stepwise modification process. The CS-Au/GCE revealed a very small semicircle domain (curve a), implying a very low electron-transfer resistance of the redox probe, because of the good conductivity of electrodeposited Au NPs. After the CS-Au/GCE was modified with HBPE-NO_2, the Rct obviously increased (curve b). This was attributed to that the self-assembled layer of HBPE-NO_2 by the electrostatic interactions and in situ chemical reaction, which was poor conductive. It's no doubt that when the electrode was conjugated with anti-AFP (curve c), AFP (curve d), subsequently, the Rct increased in succession.

Table 1
Comparison of AFP levels determined using proposed method and RECLIA.

Serum samples	Our work (ng/mL)	RECLIA (ng/mL)	Relative deviation (%)
1	323,516	319,384	1.27
2	1050	1149.14	9.44
3	8.079	8.2038	1.54
4	1419	1424.17	0.36

3.3. Analytical performance

Before evaluating the performance of proposed immunosensor, a series of conditions such as the concentration of HBPE-NO_2 NPs, incubation time, pH and scan rate were optimized in Fig. S5, results indicated that the optimized conditions were 0.1 mg/mL, 15 min, pH 7.4 and 0.1 v/s, respectively. The performance of AFP/anti-AFP/(HBPE-NO_2)/CS-Au/GCE was recorded by a series of DPVs in various concentrations of AFP solutions under the optimal experimental conditions. As a result, the amperometric response decreased with the increase of AFP concentration from 0.1 to 120 ng/mL, a linear relationship between the amperometric response and the AFP concentration was obtained with a regression equation: Y (I, μA)=191.51-1.268X (C_{AFP}, ng/mL), R^2=0.9952. The detection limit was estimated to be 0.055 ng/mL at the signal-to-noise ratio of 3, indicating that the immunesensor exhibited excellent performance compared with the reported immunesensor for detection of AFP (Table S1). The low detection limit and wide linear range may be attributed to the high specific area of Au and HBPE-NO_2 NPs, increasing the loading capacity of the anti-AFP and maintaining the activity of the immobilized anti-AFP.

3.4. Selectivity, stability and reproducibility

Selectivity is an important factor to evaluate the performance of a biosensor. In order to test the selectivity, the signal response of the prepared biosensor was assessed in various solutions containing uric acid (UA), ascorbic acid (AA), carcino embryonic antigen (CEA), β-D-(+)-Glucose (Glu), L-Glutaminic acid (L-ga), bovine serum albumin (BSA). As shown in Fig. 4B, compared with the current response caused by AFP, the signal current was almost no changed after the AFP/anti-AFP/(HBPE-NO_2)/CS-Au/GCE incubated with UA, AA, CEA, Glu, L-ga, BSA, respectively, even at high concentrations (100 ng/mL). Furthermore, the BSA/anti-AFP/(HBPE-NO_2)/CS-Au/GCE electrode was exposed to 100 ng/mL interfering antigens, separately. And the DPV current responses of the immunosensor to the high concentrations interfering antigens were shown in Fig. S6, the low current responses of interfering antigens were observed. The phenomenon indicated that the proposed biosensor had good selectivity and strong anti-interference ability in AFP detection, which can be attributed to the specific recognition between AFP and antibody and the fact that the activity of anti-AFP wasn't affected by the chemical reaction between -NH_2 (anti-AFP) and -O-COO- of HBPE-NO_2.

Stability was a powerful investigation for the development of a sensitive biosensor, it was necessary to test this for the immunosensor developed here. The electrochemical stability of proposed biosensor was investigated by CVs from −0.3 to 0.7 V over a long time (40 cycles), as shown in Fig. 4C. Encouragingly, the result exhibited strong and stable intensity without obvious descend and almost every CV curve overlapped, revealing the excellent chemical and structural stability. On the other hand, when the AFP/anti-AFP/(HBPE-NO_2)/CS-Au/GCE was stored in the refrigerator at 4 ℃ after one month the DPV response still retained 98.1% of its initial value (Fig. 4D), showing a quite satisfactory stability. Good stability can be attributed to the strong interactions between anti-AFP and AFP, and the three-dimensionally of HBPE-NO_2 modified on the electrode surface greatly enhanced the active surface available for anti-AFP binding over the HBPE-NO_2/CS-Au/GCE surface.

The reproducibility of AFP biosensor was also investigated from the DPV response (Fig. S7). Five electrodes independently fabricated were used to detect 70 ng/mL AFP, and a relative standard deviation (RSD) of 2.76% was obtained, indicating the biosensor we proposed had good electrode-to-electrode reproducibility.

3.5. Analysis of real serum samples

In order to demonstrate the analytical reliability and practical application of the proposed immunosensor, the immunosensor was used for the determination of the different concentration of AFP in human serum by standard addition methods, the calibration plot for AFP detection in serum was shown in Fig. S8. Table 1 showed the comparison between the values obtained by the proposed immunosensor and the reference values obtained by the Roche electroluminescence method (RECLIA). Experimental results indicated there was no significant difference between the two values with low relative deviation, indicating that the developed immunoassay methodology could be potentially useful for determination of AFP in biological samples.

4. Conclusion

In this case, HBPE-NO_2 NPs have been successfully synthesized by using a simple one-step method. The HBPE-NO_2 NPs possessed special architecture and properties that include high density of end-groups with negative charged, the cavity within molecules and nanosized effect. To be more specific, the HBPE-NO_2 NPs contains active ester groups on the terminal chains that can offer the in-situ chemical reaction between active ester groups and primary amine of CS and anti-AFP, and the negative Zeta-potential of HBPE-NO_2 NPs can offer the strong electrostatic interaction between nitrite group and primary amine of CS and anti-AFP. In general, it can offer electrostatic interaction, chemical reaction in-situ and large specific surface area to the fabrication of AFP biosensor. Compared to the other reported immunosensor, the novel HBPE-NO_2 NPs modified AFP biosensor had the advantages include short incubation time, simple fabrication of electrode, and the long-term stability that all attributed to the presence of the HBPE-NO_2 NPs. Therefore, the multifunctional materials such as HBP have great potential to construct novel biosensor platform with high performances and multi-functions. For example, utilizing the cavity structure of HBP and the related technique of drug loading and control release to prepare novel biosensors with detection and treatment of dual function become the target of our research group in near future.

Acknowledgements

The work was supported by National Natural Science Foundation of China (51641104, 21603105, 21571104), Chinese Postdoctoral Science Foundation (2015M580446), Jiangsu Province (1601240C), Jiangsu Key Technology RD Program (BE2016010), the Priority Academic Program Development of Jiangsu Higher Education Institution, and Major projects of Natural Sciences of University in Jiangsu Province of China (14KJA150006).

Appendix A. Supporting information

Supplementary data associated with this article can be found in the online version at doi:10.1016/j.bios.2017.01.069.

References

Ahmed, M., Narain, R., 2012. Biomaterials 33, 3990–4001.
Alpert, E., Hershberg, R., Schur, P.H., Lsselbacher, K.J., 1971. Gastroenterology 61, 137–143.
Chen, M.J., Wu, Y.S., Lin, G.F., Hou, J.Y., Li, M., Liu, T.C., 2012. Anal. Chim. Acta 741, 100–105.
Chiriacò, M.S., Feo, F.D., Primiceri, E., Monteduro, A.G., Benedetto, G.E.D., Pennetta, A., Rinaldi, R., Maruccio, G., 2015. Talanta 142, 57–63.
Cui, M., Song, Z., Wu, Y., Guo, B., Fan, X., Luo, X., 2016. Biosens. Bioelectron. 79, 736–741.
Darwish, I.A., Wani, T.A., Alanazi, A.M., Hamidaddin, M.A., Zargar, S., 2013. Talanta 111, 13–19.
Ding, D., Wang, G., Liu, J.Z., Li, K., Pu, K.Y., Hu, Y., Ng, J.C.Y., Tang, B.Z., Liu, B., 2012. Small 8, 3523–3530.
Ellinas, K., Tsougeni, K., Petrou, P.S., Bouloussis, G., Tsoukleris, D., Pavlatou, E., Tserepi, A., Kakabakos, S.E., Gogolides, E., 2016. Chem. Eng. J. 300, 394–403.
Feng, L.Y., Wu, L., Wang, J.S., Ren, J.S., Miyoshi, D., Sugimoto, N., Qu, X.G., 2012. Adv. Mater. 24, 125–131.
Gao, C., Yan, D., 2004. Prog. Polym. Sci. 29, 183–275.
Gündüz, B., Turan, N., Kaya, E., 2014. Polym. Bull. 71, 2945–2961.
Han, Q.R., Chen, X.H., Niu, Y.L., Zhao, B., Wang, B.X., Mao, C., Chen, L.B., Shen, J., 2013. Langmuir 29, 8402–8409.
Hong, H.Y., Mai, Y.Y., Zhou, Y.F., Yan, D.Y., Chen, Y., 2008. J. Polym. Sci.: Polym. Chem. 46, 668–681.
Hu, X., Ji, J., 2011. Biomacromolecules 12, 4264–4271.
Karpagam, S., Guhanathan, S., 2010. Asian J. Chem. 22, 5130–5138.
Kavosi, B., Hallaj, R., Teymourian, H., Salimi, A., 2014. Biosens. Bioelectron. 59, 389–396.
Kilic, T., Erdem, A., Erac, Y., Ozgur Seydibeyoglu, M., Okur, S., Ozsoz, M., 2015. Electroanalsis 27, 317–326.
Kolhe, P., Kannan, R.M., 2003. Biomacromolecules 4, 173–180.
Kontoyianni, C., Sideratou, Z., Theodossiou, T., Tziveleka, L.A., Tsiourvas, D., Paleos, C.M., 2008. Macromol. Biosci. 8, 871–881.
Law, W.C., Yong, K.T., Baev, A., Prasad, P.N., 2011. ACS Nano 5, 4858–4864.
Li, N., Ma, H., Cao, W., Wu, D., Yan, T., Du, B., Wei, Q., 2015. Biosens. Bioelectron. 74, 786–791.
Lu, C., Guan, C., Liu, Y., Cheng, Y., Yang, B., 2005. Chem. Mater. 17, 2448–2454.
Magnusson, H., Malmstrom, E., Hult, A., 2000. Macromolecules 33, 3099–3104.
Mucha, M., Piekielna, J., Wieczorek, A., 1999. Macromol. Symp. 144, 391–412.
Okuda, K., 1986. Dig. Dis. Sci. 31, 133–146.
Pérez-Donoso, J.M., Monrás, J.P., Bravo, D., Aguirre, A., Quest, A.F., Osorio-Román, I.O., Aroca, R.F., Chasteen, T.G., Vásquez, C.C., 2012. Plos One 7, e30741.
Pilla, V., de Lima, S.R., Andrade, A.A., Silva, A.C.A., Dantas, N.O., 2013. Chem. Phys. Lett. 580, 130–134.
Seiler, M., Jork, C., Kavarnou, A., Arlt, W., Hirsch, R., 2004. AIChE J. 50, 2439–2454.
Socrates, G., 1994. Infrared Characteristic Group Frequencies: Tables and Charts 2nd ed.. John Wiley and sons, Chichester, U.K..
Sun, C., Ma, L., Qian, Q.H., Parmar, S., Zhao, W.B., Zhao, B., Shen, J., 2014. Analyst 139, 4216–4222.
Sun, C., Wang, X.B., Yang, X.J., Xing, L., Zhao, B., Yang, X.D., Mao, C., 2013. Electrochim. Acta 106, 327–332.
Sun, D., Yang, P., Sun, H.L., Li, B.B., 2015. Eur. Polym. J. 62, 155–166.
Sun, W., Zhang, Y., Wang, X., Ju, X., Wang, D., Wu, J., Sun, Z., 2012. Electroanalysis 24, 1973–1979.
Wang, G.L., Xu, J.J., Chen, H.Y., Fu, S.Z., 2009a. Biosens. Bioelectron. 25, 791–796.
Wang, J., Zheng, Y., Nie, F., Zhai, J., Jiang, L., 2009b. Langmuir 25, 14129–14134.
Wang, X., Chen, X., Xing, L., Mao, C., Yu, H., Shen, J., 2013. J. Mater. Chem. B 1, 5036–5044.
Wang, X., Miao, J., Shao, X., Mao, C., Shen, J., 2014. J. Colloid Interf. Sci. 420, 88–96.
Wang, X.W., Xie, H., 1998. Life Sci. 64, 17–23.
Xiao, F.N., Wang, M., Wang, F.B., Xia, X.H., 2014. Small 10, 706–716.
Xie, Q.F., Weng, X.H., Lu, L.J., Lin, Z.Y., Xu, X.W., Fu, C.L., 2016. Biosens. Bioelectron. 77, 46–50.
Zagar, E., Zigon, M., Podzimek, S., 2006. Polymer 47, 166–175.
Zhou, C., Liu, D., Xu, L., Li, Q., Song, J., Xu, S., Xing, R., Song, H., 2015. Sci. Rep. 5, 9939.